

Size Constraint to Limit Interference in DRL-Free Single-Ended Biopotential Measurements

Valentin Catacora (✉ valentin.catacora@ing.unlp.edu.ar)

Universidad Nacional De La Plata Facultad de Ingenieria <https://orcid.org/0000-0002-1144-215X>

Federico Guerrero

Universidad Nacional De La Plata Facultad de Ingenieria

Enrique Spinelli

Universidad Nacional De La Plata Facultad de Ingenieria

Research Article

Keywords: Biopotential amplifier, electromagnetic interference, single-ended system, two-electrode measurement.

Posted Date: January 3rd, 2022

DOI: <https://doi.org/10.21203/rs.3.rs-1132495/v1>

License: © ⓘ This work is licensed under a Creative Commons Attribution 4.0 International License.

[Read Full License](#)

Size constraint to limit interference in DRL-free single-ended biopotential measurements

Valentín A. Catacora*, Federico N. Guerrero, and Enrique M. Spinelli

Instituto de Investigaciones en Electrónica, Control y Procesamiento de Señales LEICI (UNLP-CONICET), La Plata, Buenos Aires, Argentina

*Contact: valentin.catacora@ing.unlp.edu.ar. Tel.: +5492216197000

ORCID: 0000-0002-1144-215X; 0000-0002-7323-7872; 0000-0002-4164-9151

Abstract

Purpose: In this work, it is shown that small, battery-powered wireless devices are so robust against electromagnetic interference that single-ended amplifiers can become a viable alternative for biopotential measurements, even without a Driven Right Leg (DRL) circuit.

Methods: A power line interference analysis is presented for this case showing that this simple circuitry solution is feasible, and presenting the constraints under which it is so: small-size devices with dimensions less than 40 mm × 20 mm.

Results: A functional prototype of a two-electrode wireless acquisition system was implemented using a single-ended amplifier. This allowed validating the power-line interference model with experimental results, including the acquisition of electromyographic (EMG) signals. The prototype, built with a size fulfilling the proposed guidelines, presented power-line interference voltages below 1.2 μV_{PP} when working in an office environment.

Conclusion: It can be concluded that a single-ended biopotential amplifier can be used if a sufficiently large isolation impedance is achieved with small-size wireless devices. This approach allows measurements with only two electrodes, a very simple front-end design, and a reduced number of components.

Keywords

Biopotential amplifier; electromagnetic interference; single-ended system; two-electrode measurement.

1. Introduction

Wearable biopotential acquisition systems demand compact, light, and low-power solutions [1,2]. These devices call for simple circuits with a reduced number of parts, which at first glance would seem detrimental to their capacity to properly reject power-line interference. However, this very characteristic allows for the circuit to achieve very small physical dimensions which, in conjunction with battery-powered operation and wireless data transmission, poses the question of whether these conditions are enough to grant sufficient electromagnetic interference (EMI) robustness to the system.

Electromyography (EMG) signals are a particularly well-suited application for small, compact devices because the measurement electrodes are close to each other and can be integrated in the same device. Currently, there are many commercial battery-powered wireless sensors that meet these characteristics, such as “Trigno EMG” from Delsys. There are also EMG sensors such as “LE230” from Biometrics LTD, “FREEEMG” from BTS Bioengineering, or “PicoEMG” from Cometa, which allow high-quality EMG measurements with just two electrodes, but the specific front-end design is not widely known. The scientific works carried out in the last two decades make almost exclusive use of differential front-ends for two-electrode biopotential measurements.

The simpler the biopotential front-end, the more vulnerable it is to EMI. Three-electrode systems are more robust than their two-electrode counterparts, and differential amplifiers provide better rejection of power-line interference than single-ended (SE) topologies. Despite that, SE systems have been used to measure biopotential signals, but these are usually linked to the strategy of rejecting unwanted common-mode sources such as EMI by other means, requiring almost indispensably the use of Driven Right Leg (DRL) circuits with extra electrodes [3-8].

In this work, the focus will not be to reject interference from an SE system, but to minimize it and determine the limits up to which a device with such a simple topology can effectively measure useful biopotential signals without DRL. The disadvantages of a two-electrode SE sensor have been discussed [9-11] but, to the best of our knowledge, the physical limits of its feasibility have not been demonstrated.

In the following section we analyse the existing three- and two-electrode topologies to obtain the simplified model equations leading to the design criteria to be developed in this paper. Next, a power-line interference analysis is presented to find the conditions under which a SE amplifier can work properly, and a very simple circuit is proposed following the results of this analysis. In order to obtain experimental

results, the circuit was designed and built to be powered by batteries, transmit data wirelessly, and measure EMG signals.

2. Methods

2.1 Three-electrode systems

Traditional biopotential acquisition systems use three electrodes. Two electrodes pick-up the signal of interest employing a differential amplifier that records the potential difference between them. A third, or reference, electrode connects the patient to the amplifier DC reference (usually ground, or the average potential of the supply rails in single-supply systems). Fig. 1 shows a three-electrode system and includes the main capacitive couplings due to EMI that set the common-mode voltage v_{CM} at the amplifier's inputs [12,13]. The capacitance between the power-line and the amplifier-ground (C_{SUP}) was omitted, as accepted in the literature [3,9,14,15], because for systems with a well isolated power supply, e.g. battery-powered devices, the effect of C_{SUP} can be neglected.

The common-mode voltage v_{CM} corresponds to the potential drop across the impedance Z_{GND} of the reference electrode and is given by

$$v_{CM} = i_{ISO}Z_{GND}, \quad (1)$$

where i_{ISO} is the fraction of the displacement current i_p that flows through the isolation impedance C_{ISO} (see Fig. 1).

The main ways in which power-line interferes with the measurement are the capacitive coupling to the electrode leads, which can be mitigated using shielded wires or active electrodes, and the common-mode voltage v_{CM} [11,12]. Because of the *potential divider effect*, v_{CM} produces a differential mode voltage that is not rejected by the differential amplifier. This mode transformation involves the measuring electrode impedances Z_{E1} and Z_{E2} , and the common-mode input impedances of the amplifier Z_C . Another mode transformation is produced inside the amplifier because of its limited Common-Mode Rejection Ratio (CMRR). The total interference voltage v_{EMI} (input referenced) can be approximated by

$$v_{EMI} \approx v_{CM} \left(\frac{\Delta Z_E}{Z_C} + \frac{1}{CMRR} \right), \quad (2)$$

where $\Delta Z_E = Z_{E2} - Z_{E1}$ is the imbalance between the impedances of the measuring electrodes [11].

Another alternative for systems using three (or more) electrodes is to connect each electrode to a single-ended input, i.e. instead of connecting a pair of electrodes to a differential amplifier, each one is separately measured against a common voltage reference. Fig. 2 shows one possible topology where the measurement electrodes have been connected to such SE amplifiers. This approach is widely used, for example it is one of the possible input-multiplexer configurations of multichannel precision converters such as ADS1299 from Texas Instruments.

A SE amplifier is not able to reject common-mode voltages and its equivalent CMRR is of 0 dB [9]. If a SE amplifier is used (Fig. 3 (b)), v_{CM} appears directly at the input as biopotentials do, without any reduction or rejection, therefore:

$$v_{EMI} \approx v_{CM} = i_{ISO} Z_{GND}. \quad (3)$$

Even so, SE amplifiers have been used in multi-channel biopotential acquisition systems including some additional way to reduce v_{CM} , such as notch-filters, digital subtraction of individual channels, or both analog [16] and digital [7] DRL circuits. The DRL circuit uses negative feedback to reduce v_{CM} by a factor approximately equal to its open loop gain G_{DRL} . Hence, (3) becomes

$$v_{EMI} \approx v_{CM}/G_{DRL}. \quad (4)$$

The scheme from Fig. 2 is an example of this alternative that is well-suited for multichannel acquisition systems, since in this case it would not increase the number of electrodes significantly. This does not occur in small, portable devices such as wearable ECG monitors or EMG sensors, for which a minimum number of electrodes is desired and the measurement of biopotentials using just two electrodes is a very attractive alternative. Two-electrode systems are easy to install and comfortable, but more vulnerable to power-line interference than their three-electrode counterparts [14].

2.2 Two-electrode systems

Fig. 3 (a) shows a typical two-electrode system with a differential amplifier. In this type of topology, a relatively complex relation is established between the interference voltage and the common-mode input impedance Z_C . High values of Z_C reduce the potential divider effect, but in turn increase v_{CM} . As shown by Spinelli and Mayosky [15], the minimum v_{EMI} voltage for a given i_P is achieved for extreme values of Z_C , null or infinite, depending on ΔZ_E . For a high ΔZ_E , minimal interference is achieved for the highest

possible Z_C value, whereas for low ΔZ_E , minimal interference is achieved for the lowest possible Z_C value. In the reference, it is shown that in both cases the interference voltage v_{EMI} is given approximately by

$$v_{EMI} \approx i_{ISO} \Delta Z_E / 2. \quad (5)$$

Several circuits have been proposed to implement differential amplifiers with high [11,15,17,18] and low Z_C impedances [15,19,20]. Since these systems do not have an extra electrode to set a DC potential and provide a path for bias currents, the common-mode impedances Z_C are used instead. This imposes a trade-off between Z_C values and the input voltage-range [9], from which two approaches emerge: low Z_C strategies result in somewhat complex circuits but allow ensuring a low v_{CM} , thus preserving the amplifier input range. On the other hand, high Z_C solutions require supervising v_{CM} and taking a corrective action if it strays out of range. For example, the commercially available device MAX30003 from Maxim Integrated [18], allows selecting three different Z_C values to keep the amplifier in a proper operation point, but at the cost of degrading its interference rejection capabilities [21].

A very simple alternative to ensure a low input voltage is using a SE amplifier as Fig. 3 (b) shows. However, it has a lower rejection to power-line voltage interference than the differential amplifier approach [9]. For a two-electrode SE amplifier, the voltage v_{EMI} due to power-line effects is given by

$$v_{EMI} = i_{ISO} Z_{GND}. \quad (6)$$

Note that in this case, v_{EMI} depends on the absolute value of an electrode impedance instead of the imbalance between electrode impedances (comparing with Eq. 5). Therefore, it is a feasible alternative only if a very low i_{ISO} current can be guaranteed.

2.3 Interference model

The interference model of a two-electrode SE amplifier is shown in Fig. 3 (b). As stated above, when a SE amplifier is used the input-referred voltage due to power-line interference is given by (6). The value of the reference electrode impedance Z_{GND} depends on the type of electrode used, typically from 10 K Ω for wet electrodes to 1 M Ω and more for dry electrodes [22]. The current i_{ISO} , that flows through the isolation impedance C_{ISO} , can be obtained by analyzing the circuit of Fig. 3 (b). Considering that $C_p \ll$

C_B , the displacement current i_p to the patient can be approximated by

$$i_p \approx V_{PL} \omega_{PL} C_P = V_{PL} 2\pi f_{PL} C_P, \quad (7)$$

where V_{PL} and f_{PL} are the power-line voltage and frequency. The impedance of the reference electrode Z_{GND} is much smaller than that corresponding to C_{ISO} , so the current i_{ISO} flowing through it results

$$i_{ISO} \approx i_p \frac{1}{1+(C_{ISO}+C_B)/C_{ISO}}. \quad (8)$$

In the case of a very small device powered by batteries, C_B is much larger than C_{ISO} [23] and (8) can be approximated as:

$$i_{ISO} \approx i_p \frac{C_{ISO}}{C_B}. \quad (9)$$

Replacing (7) in (9) leads to:

$$i_{ISO} \approx V_{PL} 2\pi f_{PL} \frac{C_P C_{ISO}}{C_B}, \quad (10)$$

and v_{EMI} can be approximated by

$$v_{EMI} \approx V_{PL} 2\pi f_{PL} Z_{GND} \frac{C_P}{C_B} C_{ISO}. \quad (11)$$

Equation (11) shows that v_{EMI} responds approximately to a linear model proportional to C_{ISO} . The rest of the parameters will be considered constant in our analysis. Adopting typical values $V_{PL} = 220 V_{RMS}$; $f_{PL} = 50$ Hz; $Z_{GND} = 10$ K Ω ; $C_B = 150$ pF and a pessimistic value of $C_P = 1$ pF [23], (11) results in

$$v_{EMI} \cong 13 \frac{\mu V_{PP}}{pF} C_{ISO}. \quad (12)$$

To achieve acceptable v_{EMI} values, i.e. below the order of 10 μV_{PP} , capacitances C_{ISO} lower than 1 pF are required, which correspond to very small sized devices. As a reference, the self-capacitance of a rectangular plane is given approximately by [24]

$$C \cong \frac{2\pi\epsilon_0}{\ln(4a/b)} a, \quad (13)$$

where a and b are its dimension ($a \geq b$), and ϵ_0 the vacuum permittivity. Adopting an aspect ratio of $a/b = 2$, usual in PCB designs, (13) becomes:

$$C \cong 27 \frac{\text{pF}}{\text{m}} a. \quad (14)$$

Then, a PCB ground plane of $40 \text{ mm} \times 20 \text{ mm}$ ($a = 0.04 \text{ m}$) has a capacitance of around 1 pF. This is a rough estimate, but it allows setting the design target on devices with dimension around $40 \text{ mm} \times 20 \text{ mm}$.

2.4 Proposed circuit

The SE sensor requires an ultra-compact, wireless, and battery powered design with low energy consumption. These specifications suggest the use of an ultra-low-power general-purpose microcontroller (such as the MSP430G2553 from Texas Instruments), and a low-power wireless module (such as the HM-10 with the Bluetooth Low Energy (BLE) chip CC2541 from Texas Instruments). The analog-to-digital converter (ADC) in this microcontroller has only 10 bits of resolution (as is typical with general-purpose embedded ADCs) and its 3.3 V supply rails are its reference voltage; hence prior amplification is necessary. Therefore, the simple SE amplifier has to also include circuitry to decouple the DC potential of the electrodes and amplify the signal approximately 1000 times. In case of using a high-resolution sigma-delta technology converter this processing would not be necessary. The system will be powered by a 3.3 V single-supply source from a 3.7 V LiPo battery.

The simplest circuit for removing DC potential from the electrodes, amplifying, and bringing the signal to a reference potential consists of a passive high-pass filter followed by a non-inverting amplifier. However, it has two significant drawbacks: the first is that the input passive network degrades the input impedance of the front-end. The second is that the offset voltage and the bias current that the operational amplifier (OA) presents at the input is also amplified, and it may be of the order of millivolts, causing an undesired displacement at the output of the order of volts. Due to these drawbacks a slightly more complex circuit was implemented, guaranteeing a correct analog signal processing.

The proposed circuit is shown in Fig. 4. The design of the amplifier includes an integrator in the feedback loop responsible for eliminating the electrode's DC and the offset-compensation voltage. The gain is implemented in two stages for two reasons: the DC potential that the integrator can reject is limited by its power rails; and the divider $R_{1,2}$ amplifies the offset of the feedback OA. Given these

limitations, it is possible to design the overall gain in two stages and minimize unwanted DC potential at the amplifier output [25]. To obtain useful design parameters, the two gains are defined as

$$\alpha = \frac{R_1+R_2}{R_2}; \beta = \frac{R_3+R_4}{R_4}. \quad (15)$$

Since the DC potential to be rejected by the feedback loop OA is of the order of $\pm 300 \text{ mV}$, gain β must be less than or equal to 5.5 times so as not to exceed the 3.3 V of the supply range. Moreover, the offset of that OA will be amplified by α , so it is desirable to have the lowest possible gain at that stage, defining the values $\alpha = 200$ and $\beta = 5$.

A cut-off frequency of 5 Hz, compatible with EMG measurements, was set adjusting R_i and C_i . Note that by only modifying this cut-off frequency and lowering the gain, the same circuit can be used for ECG measurements. The signal was centered in the ADC input range by raising the amplifier's reference to the voltage V_R given by the midpoint of the power rails. As a last step, a second-order sallen-key antialiasing filter was added. All analog processing was performed with the low-power quadruple OA OPA4344 from Texas Instruments. Using this approach, the offset voltage of the feedback OA produces an acceptable DC shift of $\pm 40 \text{ mV}$.

The dominant noise source of the entire system corresponds to the voltage noise of the input OA because it is amplified by the total gain, making the other noise sources negligible if an excessively large R_4 value is avoided.

3. Results

3.1 Interference model

In order to perform experimental measurements, an EMG sensor prototype was manufactured with the design presented above, with dimensions of $40 \text{ mm} \times 20 \text{ mm}$. The device has an inter-electrode distance of 25 mm and was placed on the inner forearm using two disposable pre-gelled 3M Red Dot electrodes as Fig. 5 shows. Signals were acquired by the microcontroller at a 1 KHz sampling rate, and then transmitted over the Bluetooth link to a personal computer.

In order to validate the interference model that leads to (11), an experimental setup was prepared to measure v_{EMI} for different isolation impedances. To achieve this, different commercial capacitors (C_{LISO}) were added in parallel to the intrinsic capacitance (C_{ISO}) of the built prototype. One end of these

capacitors was soldered to a ground pad on the sensor's PCB, and the other end was connected to the earth potential. The Z_{GND} , C_P , C_B , V_{PL} and f_{PL} values can be considered invariant in this experiment. The test subject was seated on a plastic office chair in front of the computer and, with relaxed muscles, records were obtained for each capacitance value. Applying the Discrete Fourier Transform to 2-second segments of each record, an estimate of the interference voltage at 50 Hz was obtained. The experimental results of peak-to-peak interference voltage referred to the input are shown in Table 1.

Fig. 6 shows a linear least squares fit of the experimental data that allows estimating the model parameters from (11), obtaining

$$\hat{v}_{EMI} = 6.7 \mu V_{PP}/pF (C_{LISO} + C_{ISO}). \quad (16)$$

The results show a correct fit to the linear model, and additionally they reveal that capacitance C_P during the experiment corresponds to approximately half the pessimistic value proposed for (12), as reported for a subject sitting at a computer desk and using a mouse [23].

The first result in Table 1 shows that EMI during normal operation is approximately 1.2 μV_{PP} , satisfying the presented design guidelines.

3.2 Biopotential measurements

Finally, the proposed circuit was validated obtaining EMG signal records as shown in Fig. 7. The measurements consisted of two contractions of the forearm, with the electrodes positioned as shown in Fig. 5.

The sensor was comfortable, lightweight and easily adjustable by an elastic cuff. Power consumption is mainly due to the BLE module since both the microcontroller and the operational amplifiers are ultra-low power devices, allowing a small 250 mA battery to achieve more than 24 hours of continuous operation. Although the BLE module allows a long uninterrupted duration of the device, it limits movements to a very small space of no more than 10 meters to avoid losing connection.

4. Conclusions

The acquisition of biopotentials with an SE topology without rejecting sources of interference is limited by the physical dimensions of the device, but also by the impedance of the electrode. The presented

sensor was used with low impedance wet electrodes. In case of using dry electrodes, the interference will increase proportionally with the impedance as shown in equation (6).

On the other hand, it has been shown that v_{EMI} is also proportional to the relationship between the capacitances C_P and C_B (equation (11)). In this work, typical values obtained from the previous study carried out by Haberman et al [23] were considered, but it can be seen that, for the other capacitance relationships listed in that study, the interference voltage remains small.

The advantages of the designed SE sensor are its simplicity, its wireless and wearable technology, its low power consumption, and the use of low-cost and widely available commercial discrete components. These characteristics made it possible to achieve the small dimensions and the adequate interference conditions. Moreover, the total noise of the front-end can be very low since it corresponds to that of just one OA, whereas in the case of differential input instrumentation amplifiers it corresponds to at least two OAs.

Single-ended amplifiers, which have a notoriously low common-mode rejection ratio ($CMRR = 0\text{ dB}$), are a valid alternative for small-size battery-powered biopotential acquisition systems because of their very high isolation impedance. This isolation demands a wireless data transmission solution and a reduced size in order to achieve a very low C_{ISO} capacitance. The proposed scheme can be used for small battery-powered devices with dimensions less than $40\text{ mm} \times 20\text{ mm}$.

A complete wireless biopotential acquisition device based on a single-ended amplifier is proposed. It uses only two electrodes, requires a reduced number of parts, and allows acquiring high-quality biomedical signals.

References

- [1] Guk, K., Han, G., Lim, J., Jeong, K., Kang, T., Lim, E-K., Jung, J. (2019). Evolution of Wearable Devices with Real-Time Disease Monitoring for Personalized Healthcare. *Nanomaterials*, 9(6):813. <https://doi.org/10.3390/nano9060813>
- [2] Cosoli, G., Spinsante, S., Scardulla, F., D'Acquisto, L., Scalise, L. (2021). Wireless ECG and cardiac monitoring systems: State of the art, available commercial devices and useful electronic components. *Measurement*. Advance online publication. <https://doi.org/10.1016/j.measurement.2021.109243>
- [3] Winter, B. B., Webster, J. G. (1983). Driven-right-leg circuit design. *IEEE Trans Biomed Eng*, BME-30(1):62–66. <https://doi.org/10.1109/TBME.1983.325168>
- [4] Levkov, C. L. (1982). Amplification of biosignals by body potential driving. *Med Biol Eng Comput*, 20:248–250. <https://doi.org/10.1007/BF02441364>
- [5] Levkov, C. L. (1988). Amplification of biosignals by body potential driving. Analysis of the circuit performance. *Med Biol Eng Comput*, 26:389–396. <https://doi.org/10.1007/BF02442297>
- [6] Prutchi, D., Norris, M. (2005). *Design and Development of Medical Electronic Instrumentation: a practical perspective of the design, construction, and test of medical devices*. Wiley, New Jersey

- [7] Haberman, M. A., Spinelli, E. M. (2012). A Multichannel EEG Acquisition Scheme Based on Single Ended Amplifiers and Digital DRL. *IEEE Trans Biomed Circ Sys*, 6(6):614–618. <https://doi.org/10.1109/TBCAS.2012.2190733>
- [8] Biosemi. (2020). Biosemi BV: Amsterdam. Available from: <https://biosemi.com/>
- [9] Thakor, N. V., Webster, J. G. (1980). Ground-Free ECG Recording with Two Electrodes. *IEEE Trans Biomed Eng*, BME-27(12):699–704. <https://doi.org/10.1109/TBME.1980.326595>
- [10] Towe, B. C. (1981). Comments on “Ground-Free ECG Recording with Two Electrodes”. *IEEE Trans Biomed Eng*, BME-28(12):838–839. <https://doi.org/10.1109/TBME.1981.324687>
- [11] Metting van Rijn, A. C., Peper, A., Grimbergen, C. A. (1990). High-quality recording of bioelectric events – Part 1: Interference reduction, theory and practice. *Med Biol Eng Comput*, 28:389–397. <https://doi.org/10.1007/BF02441961>
- [12] Huhta, J. C., Webster, J. G. (1973). 60-Hz Interference in Electrocardiography. *IEEE Trans Biomed Eng*, BME-20(2):91–101. <https://doi.org/10.1109/TBME.1973.324169>
- [13] Metting van Rijn, A. C., Peper, A., Grimbergen, C. A. (1991). The isolation mode rejection ratio in bioelectric amplifiers. *IEEE Trans Biomed Eng*, 38(11):1154–1157. <https://doi.org/10.1109/10.99079>
- [14] Wood, D. E., Ewins, D. J., Balachandran, W. (1995). Comparative analysis of power-line interference between two- or three-electrode biopotential amplifiers. *Med Biol Eng Comput*, 33:63–68. <https://doi.org/10.1007/BF02522948>
- [15] Spinelli, E. M., Mayosky, M. A. (2005). Two-electrode biopotential measurements: power line interference analysis. *IEEE Trans Biomed Eng*, 52(8):1436–1442. <https://doi.org/10.1109/TBME.2005.851488>
- [16] Guermandi, M., Scarselli, E. F., Guerrieri, R. (2016). A driving right leg circuit (DgRL) for improved common mode rejection in bio-potential acquisition systems. *IEEE Trans Biomed Circ Sys*, 10(2):507–517. <https://doi.org/10.1109/TBCAS.2015.2446753>
- [17] Babusiak, B., Borik, S., Smondrc, M. (2020). Two-Electrode ECG for Ambulatory Monitoring with Minimal Hardware Complexity. *Sensors* 20(8):2386. <https://doi.org/10.3390/s20082386>
- [18] MAX30003 datasheet. (2020). Maxim Integrated: San Jose. Available from: <https://datasheets.maximintegrated.com/en/ds/MAX30003.pdf>
- [19] Dobrev, D., Daskalov, I. (2002). Two-electrode biopotential amplifier with current-driven inputs. *Med Biol Eng Comput*, 40:122–7. <https://doi.org/10.1007/BF02347705>
- [20] Dobrev, D. (2004). Two-electrode low supply voltage electrocardiogram signal amplifier. *Med Biol Eng Comput*, 42:272–276. <https://doi.org/10.1007/BF02344642>
- [21] Anisimov, A., Alekseev, B., Egorov, D. (2019). Development of portable cardiograph using novel front-end solutions. In: *Proceeding of the 25th Conference of Open Innovations Association (FRUCT)*, IEEE, pp. 32–37. <https://doi.org/10.23919/FRUCT48121.2019.8981497>
- [22] Rosell, J., Colominas, J., Riu, P., Pallas-Areny, R., Webster, J. G. (1988). Skin impedance from 1 Hz to 1 MHz. *IEEE Trans Biomed Eng*, 35(8):649–651. <https://doi.org/10.1109/10.4599>
- [23] Haberman, M. A., Cassino, A., Spinelli, E. M. (2011). Estimation of stray coupling capacitances in biopotential measurements. *Med Biol Eng Comput*, 49:1067–1071. <https://doi.org/10.1007/s11517-011-0811-6>
- [24] Iossel, Y. Y., Kochanov, E. S., Strunskii, M. G. (1981) *The calculation of electrical capacitance*. Energoizdat, Leningrad
- [25] Spinelli, E. M. (2014). High input impedance DC servo loop circuit. *Electron Lett*, 50(24):1808–1809. <https://doi.org/10.1049/el.2014.2262>

Statements and Declarations

This work was supported by the National Scientific and Technical Research Council (CONICET, Argentina) under Grant PIP-0558; by the La Plata National University (UNLP, Argentina) under Grants I-254 and I-014; and by the National Agency for Scientific and Technological Promotion (ANPCyT, Argentina) under Grant PICT-2018-03747.

The authors have no conflicts of interest to declare that are relevant to the content of this article.

All authors contributed to the study conception and design. Material preparation, data collection and analysis were performed by all authors. The first draft of the manuscript was written by Valentín A. Catacora and all authors commented on previous versions of the manuscript. All authors read and approved the final manuscript.

TABLE 1
EXPERIMENTAL MEASUREMENTS

C_{LISO} (pF)	0 (Without capacitor) ^a	1.2	2.2	4.7	6.8	10	12	15	22	47
V_{EMI} (μV_{pp})	1.2	10.7	18.0	31.6	53.8	61.2	80.9	96.6	159.7	315.4

Table 1. Experimental measurements. Peak-to-peak interference voltage measured for different isolation capacitances. ^aThis measurement corresponds only to the intrinsic capacitance of the device.

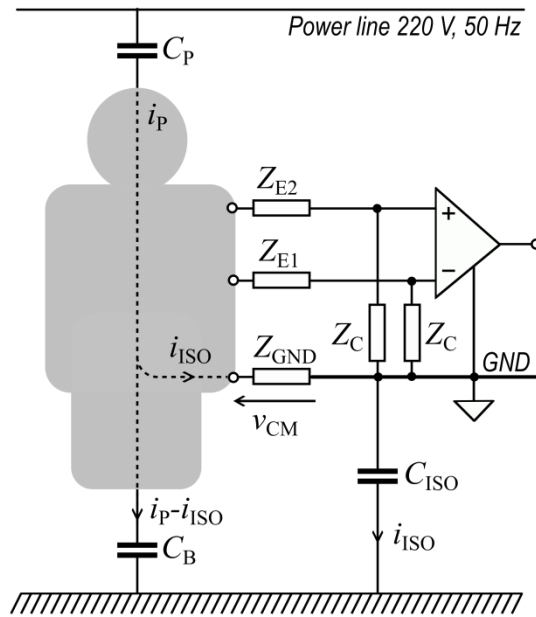


Fig. 1 Simplified interference model of a three-electrode biopotential acquisition system with a differential amplifier

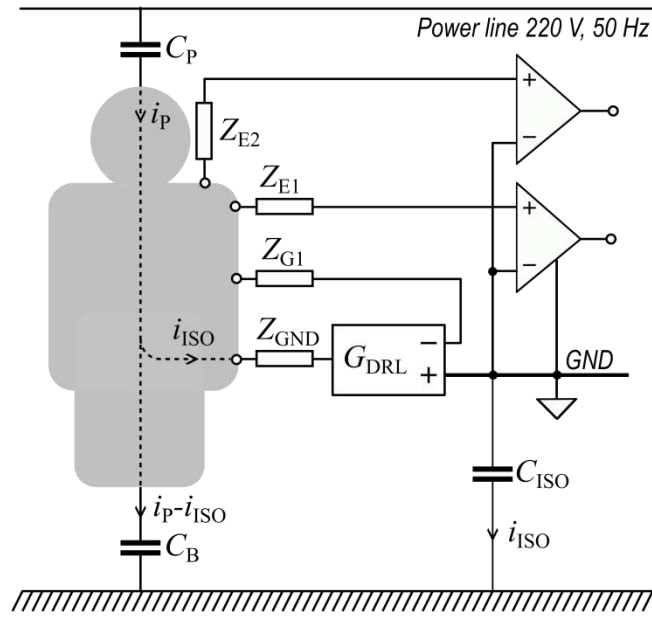


Fig. 2 Simplified interference model of a three-electrode multichannel acquisition system with Single-Ended amplifiers and Driven Right Leg circuit

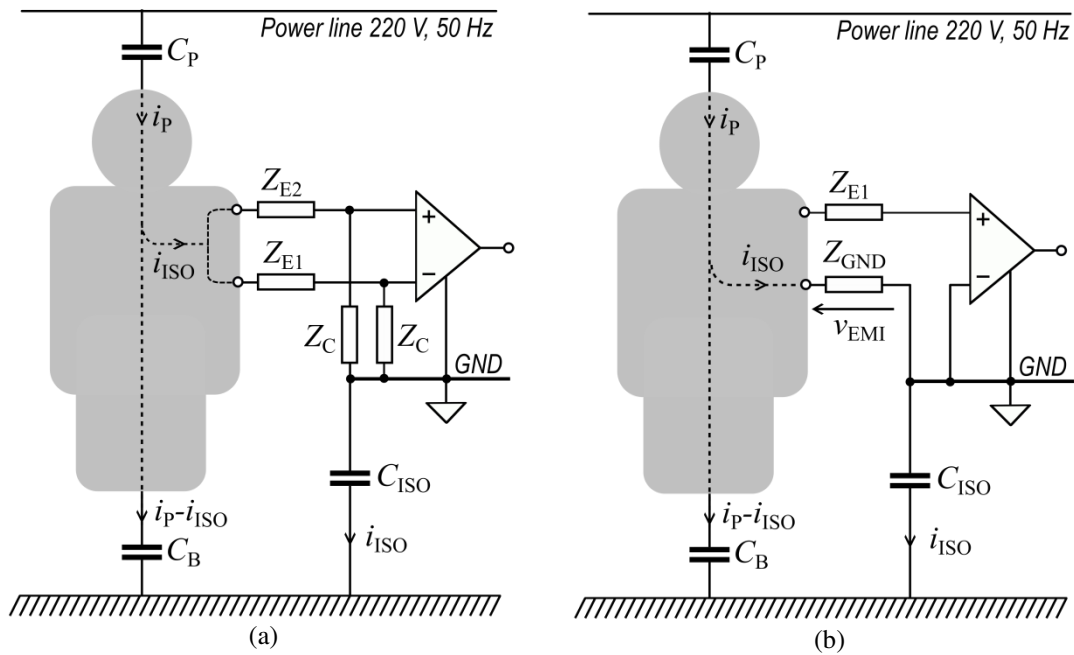


Fig. 3 Simplified interference model of a two-electrode biopotential acquisition system: (a) with a differential amplifier; (b) with a single-ended amplifier.

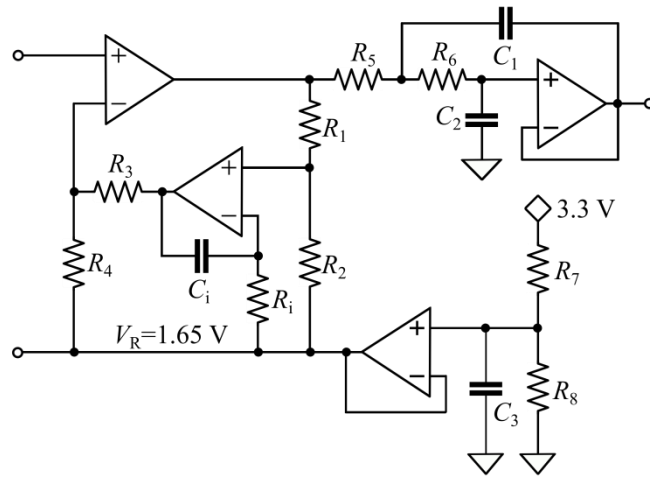


Fig. 4 Proposed Single-Ended Amplifier for EMG signals. It can be built with a quad operational amplifier device. The component values are: $R_1 = 220\text{ K}\Omega$, $R_2 = 1\text{ K}\Omega$, $R_3 = 47\text{ K}\Omega$, $R_4 = 12\text{ K}\Omega$, $R_i = 33\text{ K}\Omega$, $C_i = 1\text{ }\mu\text{F}$, $R_{5,6} = 33\text{ K}\Omega$, $C_{1,2} = 10\text{ nF}$, $R_{7,8} = 100\text{ K}\Omega$, $C_3 = 1\text{ }\mu\text{F}$. The circuit can be used for ECG signals with $R_i = 330\text{ K}\Omega$, $C_i = 10\text{ }\mu\text{F}$, and $R_1 = 180\text{ K}\Omega$

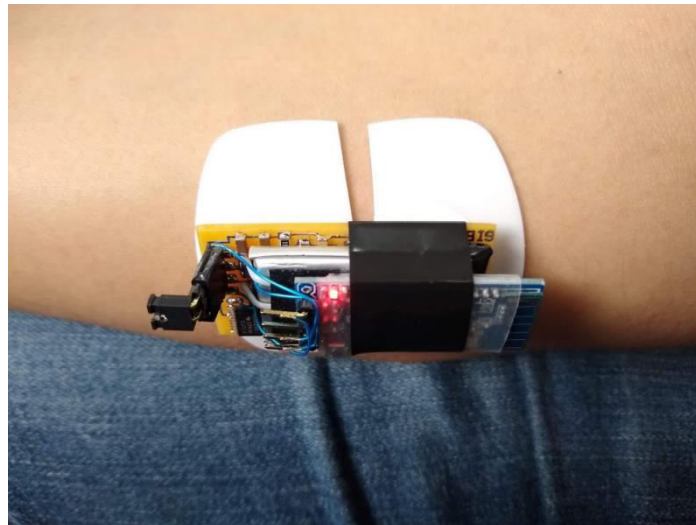


Fig. 5 Functional prototype of the device in operation

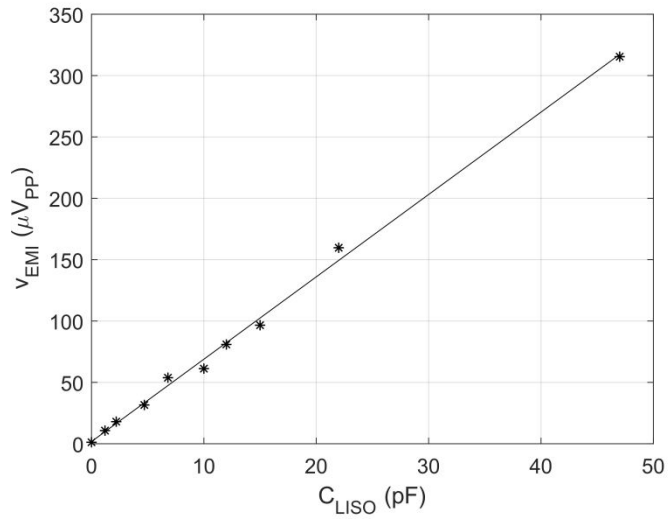


Fig. 6 Interference voltage as a function of the additional capacitance C_{LISO}

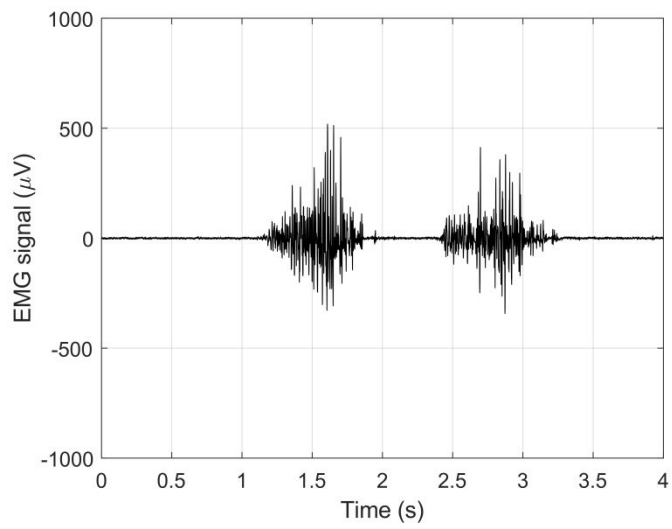


Fig. 7 EMG signal acquired with the SE device referred to the input